Impact of Flux Gate Location on Antarctic Mass Balance via Input-Output Method

Yixiang Tian [1,2], Shuwei Jia [1,2]

[1] College of Surveying and Geo-Informatics, Tongji University, 1239 Siping Road, Shanghai, China – tianyixiang@tongji.edu.cn, 2433859@tongji.edu.cn
[2] Center for Spatial Information Science and Sustainable Development Applications, Tongji University, 1239 Siping Road, Shanghai,China

Keywords: Antarctic ice sheet, Flux gate, Mass balance, Input-output.

Abstract

In the context of global warming, studies have shown that the Antarctic Ice Sheet (AIS) has been experiencing continuous mass loss, constituting a significant contribution to global sea level rise. Utilizing an optimized input-output method (IOM), this study evaluates the 2013~2022 mass balance of eight widely studied Antarctic drainage basins. By integrating RACMO2.4 surface mass balance (SMB), BedMachine ice thickness, and ITS_LIVE annual velocity, we quantify the sensitivity of mass balance estimates to flux gate (FG) location. Results demonstrate that while flux estimates along disparate radar tracks vary by <4%, discrepancies between grounding line and flight-line-based gates can reach 20%, highlighting the importance of flux gate selection. Regional assessments reveal a pronounced regime shift in East Antarctica: basins previously in near-balance or slight loss—including the Amery region and Basins 12~13—transitioned to significant mass accumulation post-2020, primarily driven by a sharp increase in SMB. In contrast, the Amundsen Sea sector in West Antarctica exhibited sustained and accelerating mass loss, with net deficits increasing from –163.9±15.3 Gt a^{-1} (2013~2019) to -179.2±15.5 Gt a^{-1} (2020~2022). This divergence stems from the dominance of anomalous precipitation in the East versus persistent ice flux acceleration in the West.

1. Introduction

The Antarctic Ice Sheet (AIS), the largest terrestrial ice mass on Earth, contains approximately 90% of the planet's total ice volume. Its complete melting would trigger a global sea-level rise of about 57 meters (IPCC, 2023; The IMBIE team, 2018). Long-term research results indicate that the AIS is undergoing continuous mass loss. According to the comprehensive assessment results of mass balance, the AIS lost a total of 2670±870 Gt of ice between 1992 and 2020, with a mass loss rate of 95±31 Gt a^{-1} (Otosaka et al., 2023). During the period 1992~1999, the average mass loss rate was estimated at 49±51 Gt a^{-1}. The lost rate increased to 70±48 Gt a^{-1} during 2000~2009, and further accelerated to 148±54 Gt a^{-1} between 2010 and 2016.

At present, a variety of monitoring methods have been widely employed in the study of ice sheet mass balance, including the input-output method (IOM), satellite gravimetry method, and satellite altimetry method (Rignot et al., 2019; Smith et al., 2020; Velicogna et al., 2020). Altimetry method determines ice sheet mass changes by repeatedly acquiring surface elevation measurements over the same region based on laser altimetry satellites (e.g., ICESat and ICESat-2) or radar altimetry satellites (e.g., ERS-1/2, Envisat, CryoSat-2). Changes in surface elevation over time are computed, and, by incorporating the area of the monitored region along with the density of ice and snow, volume and mass variations within the region can be estimated (Aublanc et al., 2018; Flament and Rémy, 2012; Shepherd et al., 2019; Zwally et al., 2015). The gravimetry method estimates ice sheet mass changes by converting the monthly time-variable gravity observations provided by gravity satellites (e.g., GRACE and GRACE-FO) into spherical harmonic coefficients, which are then transformed into equivalent water height, allowing for the quantification of mass variations in the ice sheet (Velicogna et al., 2020). The input-output method estimates the mass balance of the AIS by calculating the difference between mass input and mass output. The input component, which includes mass gain from snowfall and losses from sublimation, meltwater runoff, and surface melting, is primarily quantified through the surface mass balance (SMB). This is typically derived using regional climate models and reanalysis datasets, such as RACMO (Van Wessem et al., 2018, 2014), MAR (Agosta et al., 2019), and ERA (Hersbach et al., 2020). The primary output component is ice discharge across the grounding line, quantified using surface ice velocity, ice thickness, and grounding line position data (Gardner et al., 2018; Rignot et al., 2019). Therefore, Input-output method, as one of the three primary techniques for monitoring Antarctic ice sheet mass balance, is constrained by the accuracy of data on ice thickness, ice flow velocity, and surface mass balance. This results in substantial uncertainty in assessments of Antarctic ice sheet mass balance, particularly in regions such as the Antarctic Peninsula and East Antarctica, where uncertainty can reach as high as 51% (Davison et al., 2025).

In recent years, the continuous release of high-quality ice velocity and ice thickness datasets has significantly enhanced the accuracy of AIS mass balance estimates. The annual ice velocity product ITS_LIVE, published by Gardner et al, provides high-resolution data at 120 m and 240 m. In addition, the latest ice thickness dataset, BedMachine V3, with a spatial resolution of 500 m, provides high-precision ice thickness information (Morlighem et al., 2020). Moreover, the appropriate selection of flux gates is crucial for reliable mass balance estimates. Currently, two main approaches are employed to define flux gates: one directly employs the grounding line as the flux gate (Lin et al., 2023), while the other shifts the flux gate inland to regions where high-quality ice thickness data exist (Gardner et al., 2018; Rignot et al., 2019). The former generally introduces higher uncertainty in the estimated ice flux, whereas the latter effectively reduces this uncertainty but makes the final results more sensitive to the applied surface mass-balance corrections.

This study refines the input-output framework by integrating the latest remote sensing data products and improving the location of flux gates, thereby enhancing the accuracy of mass-balance estimates.

2. Study areas and Data

2.1 Study areas

We selected eight widely studied Antarctic drainage basins for analysis, including Basins 9~13 in East Antarctica and Basins 20~22 in West Antarctica (Figure 1). Basins 9~11 are located in Amery region and exhibit relatively stable mass balance, whereas Basins 12 (Queen Mary Land) and 13 (Wilkes Land) dominate regional mass loss. In West Antarctica, Basins 20~22 drive the continent's most severe mass depletion. Ice velocities across these regions span a wide range, from slow to extremely fast, and their spatial distribution provides a robust framework for evaluating ice discharge and its associated uncertainties.

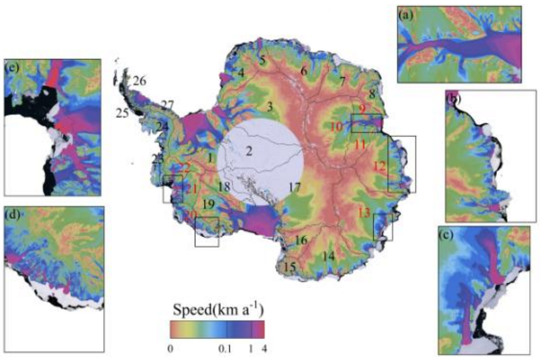

Figure 1. Study area: (a) Basin 9~11, (b) Basin 12, (c) Basin 13, (d) Basin 20, (e) Basin 21, 22.The base map is the Landsat Image Mosaic of Antarctica (LIMA), and the background ice velocity is derived from the ITS_LIVE annual ice velocity of 2015 (Gardner et al., 2018).

2.2 Data

In this study, we integrated multiple state-of-the-art datasets, including the high-resolution annual ice velocity maps from ITS_LIVE V2, the ice thickness product BedMachine V3, and the latest surface mass balance data from RACMO2.4p1 (Gardner et al., 2018; Morlighem et al., 2020; Van Dalum et al., 2024). Detailed information about the data is provided in Table 1.

Surface Mass Balance (SMB): We utilized regional climate models RACMO2.3p2 and RACMO2.4p1. RACMO2.3p2 offers 27 km resolution (5.5 km over the Peninsula) with monthly data over 1979~2022, which captures stronger coastal interannual correlations. The latest RACMO2.4p1 provides monthly outputs (1979~2023) at a refined 11 km resolution, demonstrating enhanced overall simulation performance for key climatic parameters (Van Dalum et al., 2024).

Ice Flow Velocity: Surface velocities were derived from the ITS_LIVE Version 2 annual mosaics (Gardner et al., 2018). Processed via the autoRIFT algorithm from Landsat imagery, this product provides near-complete AIS coverage from 2013 onwards. Its 120 m spatial resolution is optimal for precise, large-scale basin discharge calculations.

Ice Thickness: We employed BedMachine V3 (500 m resolution), which synthesizes airborne radar sounding (RES) data, InSAR velocities, and Reference Elevation Model of Antarctica (REMA) topography using mass conservation and streamline diffusion (Morlighem et al., 2020). Thickness uncertainty is tightly constrained (< 30 m) along RES flight lines but increases in interpolated regions.

Boundaries and Flux Gates: The grounding line was established using a MEaSUREs/ASAID composite (Bindschadler et al., 2011; Rignot et al., 2019). In addition, we also utilized the FG2 flux gate configuration (Gardner et al., 2018), which strategically shifts the flux gate inland to align with highly accurate RES flight lines.

Data type	Dataset	Time period
Ice velocity	ITS_LIVE V1	2013~2018
	ITS_LIVE V2	2013~2022
Ice thickness	BedMachine V3	1970~2019
Grounding line	MEaSUREs	1992~2014
Flux gates	FG2	1992~2013
SMB	RACMO2.3p2	1979~2022
	RACMO2.4p1	1979~2023

Table 1. Detailed information of the used data

3. Method

3.1 Calculation method for mass balance

The mass balance of each drainage basin was calculated using the following equation:

$$MB = SMB - \text{Discharge} \tag{1}$$

To account for significant interannual variability, this study uses monthly RACMO2.4p1 data (2013~2022) to ensure a high-fidelity representation of mass changes.

Ice discharge is the mass of ice flowing across the grounding line per unit time. It is calculated by establishing a flux gate (FG) along a discretized grounding line, where each segment of length ds extends vertically through the ice thickness H. Total basin discharge is the aggregate flux of all segments, computed via equation (2):

$$\text{Flux} = \sum_{i=1}^{n} (vx_i dy_i + vy_i dx_i) H_i \rho_{ice} \tag{2}$$

In equation (2), the unit segment is projected onto the x and y axes as dx_i and dy_i, respectively. Similarly, the ice velocity is resolved into its x and y components, vx_i and vy_i. H_i denotes the ice thickness at the i-th segment, and ρ_{ice} represents the ice density, typically assumed to be 917 kg m^{-3}. To accurately represent ice discharge at the grounding line, a correction term, $Corr_{FG-GL}$, must be applied to the FG calculation. This correction accounts for SMB, basal melt, and dynamic volume change within the region bounded by the FG and the grounding line. Given that SMB constitutes ~95% of this correction (Gardner et al., 2018), it is calculated with the specific polygon enclosed by the FG, grounding line, and basin boundary. Using RACMO2.4p1 data, the corrected discharge is expressed as follows:

$$\text{Discharge} = \text{Flux} + Corr_{FG-GL} \tag{3}$$

3.2 Assessment of uncertainty in mass balance

When calculating ice flux across the FG, the primary sources of uncertainty are from ice thickness and ice velocity. Therefore, the ice flux uncertainty can be derived from equation (2) based on the law of error propagation, resulting in equation (4):

$$\sigma_{\text{Flux}} = \rho\sqrt{\sum_{i=1}^{n}\left[(vx_i dy_i + vy_i dx_i)^2 \sigma_{H_i}^2 + H_i^2 (dy_i^2 \sigma_{vx_i}^2 + dx_i^2 \sigma_{vy_i}^2)\right]} \quad (4)$$

Where σ_{Hi} denotes the uncertainty of ice thickness Hi, while σ_{vxi} and σ_{vyi} represent the uncertainties in ice velocity in the x and y directions at the same unit. Further simplification of equation (4) leads to equation (5)

$$\sigma_{\text{Flux}} = \sqrt{\sum_{i=1}^{n} \text{Flux}_i^2 \left(\frac{\sigma_{H_i}^2}{H_i^2} + \frac{\sigma_{vx_i}^2}{vx_i^2} + \frac{\sigma_{vy_i}^2}{vy_i^2}\right)} \quad (5)$$

To determine the total ice discharge uncertainty at the grounding line, the correction term uncertainty $\sigma_{\text{CorrFG-GL}}$ must be incorporated. Assuming statistical independence between the flux uncertainty and the correction term uncertainty, the combined uncertainty is derived as follows:

$$\sigma_{\text{Discharge}} = \sqrt{\left(\sigma_{\text{Flux}}^2 + \sigma_{Corr_{FG-GL}}^2\right)} \quad (6)$$

The uncertainty of correction term, $\sigma_{\text{CorrFG-GL}}$, is derived from the uncertainty of the SMB within the region between the FG and the grounding line. Finally, the uncertainty in mass balance for each basin is calculated using the following equation:

$$\sigma_{MB} = \sqrt{\left(\sigma_{SMB}^2 + \sigma_{\text{Discharge}}^2\right)} \quad (7)$$

3.3 Data Preprocessing and Experimental Design

We utilized monthly RACMO2.4p1 (2013~2022) for SMB calculation due to its superior performance over RACMO2.3 (Van Dalum et al., 2024). Lacking native uncertainty fields, conservative SMB error estimates were derived using the elevation-dependent function from RACMO2.3p2 (Van Wessem et al., 2018) and RAMP DEM topography. Ice velocity data from ITS_LIVE V1 (2013~2018) were extended to 2022 using V2, with gaps infilled via contemporaneous V1 and adjacent V2 data to ensure flux completeness. To address anomalous V2 uncertainty fields in Basins 12~13 and 20~22, we substituted them with V1-derived uncertainty values—applying direct V1 estimates for the 2013~2018 period and utilizing the 2013~2018 average as a proxy for 2019~2022. Given that ice thickness remains the dominant source of error (Morlighem et al., 2020), we assessed three flux gate (FG) locations (Figure 2): GL/FG0 (along the grounding line), FG1 (positioned where thickness uncertainty < 30 m via BedMachine V3), and FG2 (Gardner et al., 2018).

This study estimates ice discharge and associated uncertainties for experimental basins, and analyzes the impact of gate placement. Based on the result, we introduce a flux gate placement strategy that balances proximity to the grounding line against uncertainty reduction. Finally, ice discharge and its uncertainty are reevaluated for experimental basins using the optimized flux gate location.

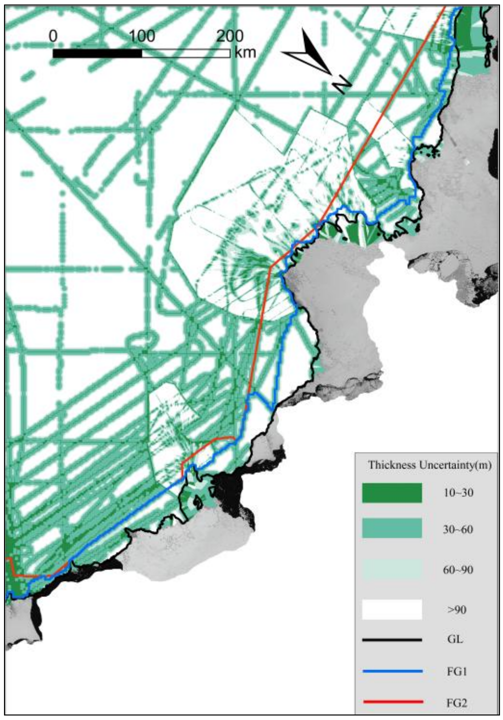

Figure 2. Spatial distribution of BedMachine ice thickness uncertainties, airborne radar tracks and flux gates of Basin 12.

4. Result

4.1 Ice discharge uncertainty along grounding line

The baseline grounding-line flux gate (FG0) was discretized and stratified by ice velocity for analyzing the impact of ice thickness and ice velocity uncertainties on ice flux uncertainty as shown in Figure 3. Although ice thickness uncertainty generally dominates, velocity uncertainty becomes the primary uncertainty source in low-velocity region, specifically in areas of the Amery where ice velocity is below 30 m a^{-1}. Consequently, the common practice of shifting flux gates inland to align with RES flight lines—intended to minimize ice thickness uncertainty—increases the uncertainty of correction terms, thereby proving counterproductive in these areas. Therefore, this study proposes a velocity-dependent FG configuration strategy: in high-velocity regions, the FG is aligned with RES transects to prioritize thickness accuracy; in low-velocity regions, the FG is positioned near the grounding line to minimize correction errors, as ice thickness uncertainty and ice velocity uncertainty are comparable and total uncertainty is relatively low. Using a ratio threshold of 1.5 (derived from Figure 3), we optimized the original configuration into new FG1, which serves as the basis for all subsequent results.

4.2 Ice discharge and changes for basins from 2013 to 2022

To evaluate the influence of FG configurations on ice discharge magnitude, we compared three sets of gates (FG0, FG1, FG2) across basins 9~13 and 20~22. While interannual variability remained consistent across all configurations, significant discrepancies in absolute discharge were observed. Specifically, grounding-line estimates (FG0) were systematically lower than those from RES-aligned gates (FG1 and FG2), with maximum deviations of 8.5%, 7.4%, and 19.5% in basins 12, 13, and 20, respectively. The discrepancy between FG0—defined along the grounding line—and FG1 or FG2 can reach up to 20%. In contrast, FG1 and FG2 estimates—both leveraging reliable thickness measurements—differed by less than 4%. Analysis of FG1 results (2013~2022) indicates relative stability in East Antarctica and West Antarctica's basin 20. Conversely, basins 21 and 22 showed sustained growth, each averaging an increase of 1.9 Gt a^{-1}. From an error-propagation perspective, FG1 significantly outperformed FG0 by minimizing thickness uncertainty. For instance, in the Amery sector, 75% of FG1 segments maintained σH < 30m, compared to only 21% for FG0. However, regional performance varied; while FG1 generally minimized uncertainty, FG2 was superior in basin 13. This suggests that while reducing ice thickness uncertainty is critical, the total uncertainty is a combined function of discharge magnitude, ice thickness uncertainty, and ice velocity uncertainty.

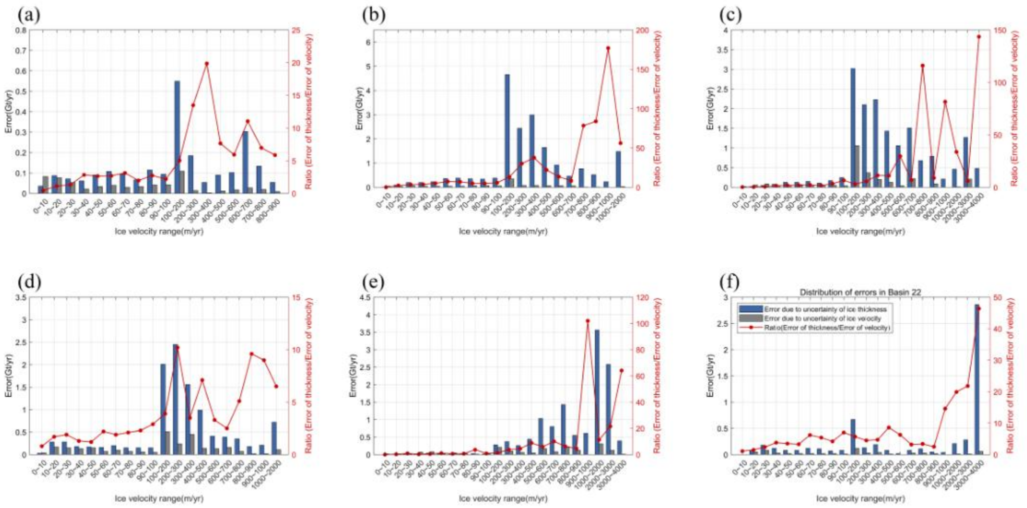

Figure 3. Ice flux uncertainty results from ice thickness uncertainty and ice velocity uncertainty across different velocity ranges in the experimental basins: The blue columns represent the uncertainty caused by ice thickness data for all flux gate units within each ice flow velocity range; The black columns represent the uncertainty caused by ice flow velocity data for all fluxgate units within each ice flow velocity range.

4.3 Mass balance and changes for basins

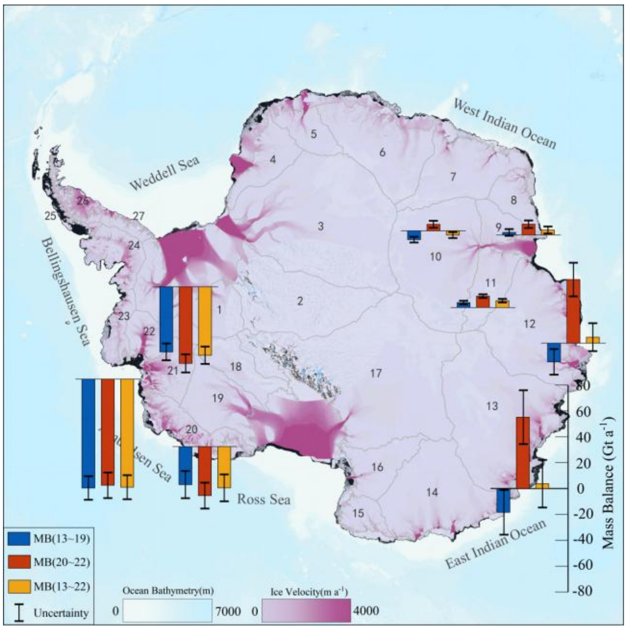

Figure 4. Mass balance of the experimental basins from 2013 to 2022: mass balance for 2013~2019 (blue), 2020~2022 (red), and 2013~2022 (yellow).

Figure 4 illustrates the mass balance evolution of Antarctic basins 12, 13, 20 and 22 from 2013 to 2022. During the 2013~2019 period, basins 12 and 13 in East Antarctica experienced substantial mass loss, while basins 20 and 22 likewise exhibited pronounced negative mass balance, confirming these regions as major contributors to Antarctica's net mass loss. During 2020~2022, enhanced precipitation led to widespread positive surface mass balance anomalies across East Antarctica, with the most prominent increases observed in the Amery, Queen Mary, and Wilkes Land regions. In contrast, changes across West Antarctic basins were comparatively minor. As a result, basins 12 and 13 shifted from persistent mass loss to substantial mass gain during this period. Meanwhile, the Amundsen Sea sector continued to experience severe mass loss, further intensified by ongoing increases in ice discharge. Overall, the anomalous mass accumulation across Antarctica during 2020~2022 effectively moderated the ice sheet's contribution to global sea-level rise.

5. Conclusion

This study investigates the impact of flux gate selection on the estimation of ice flux and its associated uncertainty using the input-output method. It discusses the respective effects of ice velocity and ice thickness uncertainties on the overall uncertainty of ice flux estimation and proposes a new method for defining flux gates. The results indicate that the difference in estimated ice flux between flux gates based on observational data is less than 4%, while the deviation can reach up to approximately 20% when comparing flux gates based directly on the grounding line with those derived from observations. According to the mass balance results in this study, the entire Amery region remained in a slightly negative balance during 2013~2019, with basins 12 and 13 experiencing substantial mass loss, reaching -14.4 ±9.8 Gt a^{-1} and -18.4±17.3 Gt a^{-1}, respectively. Notably, following a prolonged period of mass loss, these basins exhibited mass gain during 2020~2022. The accumulation rate for the entire Amery region during this period reached 22.2±3.9 Gt a^{-1}, while basins 12 and 13 reached

49.2±12.9 Gt a^{-1} and 55.1±20.8 Gt a^{-1}, respectively. In contrast, West Antarctica showed an accelerating trend in mass loss during 2013~2022. Specifically, basins 20 to 22 in the Amundsen Sea sector exhibited an increase in ice flux at a rate of 3.3±1.1 Gt a^{-1}, with an overall mass balance of -168.4±15.4 Gt a^{-1}.

Acknowledgements

We would like to thank the National Snow and Ice Data Center (NSIDC) for providing MEaSUREs ice flow velocity data, ITS_LIVE ice flow velocity data, and BedMachine ice thickness data. This work was supported by the Natural Science Foundation of China under Grant 42394131.

References

Agosta, C., Amory, C., Kittel, C., Orsi, A., Favier, V., Gallée, H., Van Den Broeke, M.R., Lenaerts, J.T.M., Van Wessem, J.M., Van De Berg, W.J., Fettweis, X., 2019. Estimation of the Antarctic surface mass balance using the regional climate model MAR (1979–2015) and identification of dominant processes. The Cryosphere 13, 281–296. doi.org/10.5194/tc-13-281-2019

Aublanc, J., Moreau, T., Thibaut, P., Boy, F., Rémy, F., Picot, N., 2018. Evaluation of SAR altimetry over the antarctic ice sheet from CryoSat-2 acquisitions. Advances in Space Research 62, 1307–1323. doi.org/10.1016/j.asr.2018.06.043

Bindschadler, R., Choi, H., Wichlacz, A., Bingham, R., Bohlander, J., Brunt, K., Corr, H., Drews, R., Fricker, H., Hall, M., Hindmarsh, R., Kohler, J., Padman, L., Rack, W., Rotschky, G., Urbini, S., Vornberger, P., Young, N., 2011. Getting around Antarctica: new high-resolution mappings of the grounded and freely-floating boundaries of the Antarctic ice sheet created for the International Polar Year. The Cryosphere 5, 569–588. doi.org/10.5194/tc-5-569-2011

Davison, B.J., Hogg, A.E., Slater, T., Rigby, R., Hansen, N., 2025. Antarctic Ice Sheet grounding line discharge from 1996–2024. Earth Syst. Sci. Data 17, 3259–3281. doi.org/10.5194/essd-17-3259-2025

Flament, T., Rémy, F., 2012. Dynamic thinning of Antarctic glaciers from along-track repeat radar altimetry. J. Glaciol. 58, 830–840. doi.org/10.3189/2012jog11j118

Gardner, A.S., Moholdt, G., Scambos, T., Fahnstock, M., Ligtenberg, S., Van Den Broeke, M., Nilsson, J., 2018. Increased West Antarctic and unchanged East Antarctic ice discharge over the last 7 years. The Cryosphere 12, 521–547. doi.org/10.5194/tc-12-521-2018

Hersbach, H., Bell, B., Berrisford, P., Hirahara, S., Horányi, A., Muñoz-Sabater, J., Nicolas, J., Peubey, C., Radu, R., Schepers, D., Simmons, A., Soci, C., Abdalla, S., Abellan, X., Balsamo, G., Bechtold, P., Biavati, G., Bidlot, J., Bonavita, M., De Chiara, G., Dahlgren, P., Dee, D., Diamantakis, M., Dragani, R., Flemming, J., Forbes, R., Fuentes, M., Geer, A., Haimberger, L., Healy, S., Hogan, R.J., Hólm, E., Janisková, M., Keeley, S., Laloyaux, P., Lopez, P., Lupu, C., Radnoti, G., De Rosnay, P., Rozum, I., Vamborg, F., Villaume, S., Thépaut, J., 2020. The ERA5 global reanalysis. Quart J Royal Meteoro Soc 146, 1999–2049. doi.org/10.1002/qj.3803

IPCC, 2023. Climate Change 2021 – The Physical Science Basis: Working Group I Contribution to the Sixth Assessment Report of the Intergovernmental Panel on Climate Change, 1st ed. Cambridge University Press. doi.org/10.1017/9781009157896

Lin, Y., Yu, Z., Liu, Y., Chen, X., Shen, Q., Zhao, L., 2023. Assessment of Antarctic Ice Sheet mass balance from 2005 to 2016. National Remote Sensing Bulletin 27, 318–334. doi.org/10.11834/jrs.20210446

Morlighem, M., Rignot, E., Binder, T., Blankenship, D., Drews, R., Eagles, G., Eisen, O., Ferraccioli, F., Forsberg, R., Fretwell, P., Goel, V., Greenbaum, J.S., Gudmundsson, H., Guo, J., Helm, V., Hofstede, C., Howat, I., Humbert, A., Jokat, W., Karlsson, N.B., Lee, W.S., Matsuoka, K., Millan, R., Mouginot, J., Paden, J., Pattyn, F., Roberts, J., Rosier, S., Ruppel, A., Seroussi, H., Smith, E.C., Steinhage, D., Sun, B., Broeke, M.R.V.D., Ommen, T.D.V., Wessem, M.V., Young, D.A., 2020. Deep glacial troughs and stabilizing ridges unveiled beneath the margins of the Antarctic ice sheet. Nat. Geosci. 13, 132–137. doi.org/10.1038/s41561-019-0510-8

Otosaka, I.N., Shepherd, A., Ivins, E.R., Schlegel, N.-J., Amory, C., Van Den Broeke, M.R., Horwath, M., Joughin, I., King, M.D., Krinner, G., Nowicki, S., Payne, A.J., Rignot, E., Scambos, T., Simon, K.M., Smith, B.E., Sørensen, L.S., Velicogna, I., Whitehouse, P.L., A, G., Agosta, C., Ahlstrøm, A.P., Blazquez, A., Colgan, W., Engdahl, M.E., Fettweis, X., Forsberg, R., Gallée, H., Gardner, A., Gilbert, L., Gourmelen, N., Groh, A., Gunter, B.C., Harig, C., Helm, V., Khan, S.A., Kittel, C., Konrad, H., Langen, P.L., Lecavalier, B.S., Liang, C.-C., Loomis, B.D., McMillan, M., Melini, D., Mernild, S.H., Mottram, R., Mouginot, J., Nilsson, J., Noël, B., Pattle, M.E., Peltier, W.R., Pie, N., Roca, M., Sasgen, I., Save, H.V., Seo, K.-W., Scheuchl, B., Schrama, E.J.O., Schröder, L., Simonsen, S.B., Slater, T., Spada, G., Sutterley, T.C., Vishwakarma, B.D., Van Wessem, J.M., Wiese, D., Van Der Wal, W., Wouters, B., 2023. Mass balance of the Greenland and Antarctic ice sheets from 1992 to 2020. Earth Syst. Sci. Data 15, 1597–1616. doi.org/10.5194/essd-15-1597-2023

Rignot, E., Mouginot, J., Scheuchl, B., Van Den Broeke, M., Van Wessem, M.J., Morlighem, M., 2019. Four decades of Antarctic Ice Sheet mass balance from 1979–2017. Proc. Natl. Acad. Sci. U.S.A. 116, 1095–1103. doi.org/10.1073/pnas.1812883116

Shepherd, A., Gilbert, L., Muir, A.S., Konrad, H., McMillan, M., Slater, T., Briggs, K.H., Sundal, A.V., Hogg, A.E., Engdahl, M.E., 2019. Trends in Antarctic Ice Sheet Elevation and Mass. Geophysical Research Letters 46, 8174–8183. doi.org/10.1029/2019gl082182

Smith, B., Fricker, H.A., Gardner, A.S., Medley, B., Nilsson, J., Paolo, F.S., Holschuh, N., Adusumilli, S., Brunt, K., Csatho, B., Harbeck, K., Markus, T., Neumann, T., Siegfried, M.R., Zwally, H.J., 2020. Pervasive ice sheet mass loss reflects competing ocean and atmosphere processes. Science 368, 1239–1242. doi.org/10.1126/science.aaz5845

The IMBIE team, 2018. Mass balance of the Antarctic Ice Sheet from 1992 to 2017. Nature 558, 219–222. doi.org/10.1038/s41586-018-0179-y

Van Dalum, C.T., Van De Berg, W.J., Gadde, S.N., Van Tiggelen, M., Van Der Drift, T., Van Meijgaard, E., Van Ulft, L.H., Van Den Broeke, M.R., 2024. First results of the polar regional climate model RACMO2.4. The Cryosphere 18, 4065–4088. doi.org/10.5194/tc-18-4065-2024

Van Wessem, J.M., Reijmer, C.H., Morlighem, M., Mouginot, J., Rignot, E., Medley, B., Joughin, I., Wouters, B., Depoorter, M.A., Bamber, J.L., Lenaerts, J.T.M., Van De Berg, W.J., Van Den Broeke, M.R., Van Meijgaard, E., 2014. Improved representation of East Antarctic surface mass balance in a regional atmospheric climate model. J. Glaciol. 60, 761–770. doi.org/10.3189/2014jog14j051

Van Wessem, J.M., Van De Berg, W.J., Noël, B.P.Y., Van Meijgaard, E., Amory, C., Birnbaum, G., Jakobs, C.L., Krüger, K., Lenaerts, J.T.M., Lhermitte, S., Ligtenberg, S.R.M., Medley, B., Reijmer, C.H., Van Tricht, K., Trusel, L.D., Van Ulft, L.H., Wouters, B., Wuite, J., Van Den Broeke, M.R., 2018. Modelling the climate and surface mass balance of polar ice sheets using RACMO2 – Part 2: Antarctica (1979–2016). The Cryosphere 12, 1479–1498. doi.org/10.5194/tc-12-1479-2018

Velicogna, I., Mohajerani, Y., A, G., Landerer, F., Mouginot, J., Noel, B., Rignot, E., Sutterley, T., Van Den Broeke, M., Van Wessem, M., Wiese, D., 2020. Continuity of Ice Sheet Mass Loss in Greenland and Antarctica From the GRACE and GRACE Follow-On Missions. Geophysical Research Letters 47. doi.org/10.1029/2020gl087291

Zwally, H.J., Li, J., Robbins, J.W., Saba, J.L., Yi, D., Brenner, A.C., 2015. Mass gains of the Antarctic ice sheet exceed losses. J. Glaciol. 61, 1019–1036. doi.org/10.3189/2015jog15j071